The Role of Colloidal Quantum Dots Capping Ligands in Photocatalytic Lignin Valorization

Elio Rico[a], Xavier Marset[a], Francisco J. Pastor [b], Salvador Montilla-Verdú[a], Wu Lan [c], Liang Yao[d], Néstor Guijarro[a],*

[a] Institute of Electrochemistry, Universidad de Alicante, Apdo. 99, 03080 Alicante, Spain.

[b] Departament de Química Física, Apartat 99, E-03080 Alacant, Spain

[c] State Key Laboratory of Pulp and Paper Engineering, South China University of Technology, Guangzhou 510640, China

[d] State Key Laboratory of Luminescent Materials and Devices, Institute of Polymer Optoelectronic Materials and Devices, Guangdong Basic Research Center of Excellence for Energy and Information Polymer Materials South China University of Technology, Guangzhou 510640, China

Abstract

The efficient transformation of biomass into high-value chemicals remains a significant challenge, with surface ligand manipulation offering a promising approach to enhance catalytic performance. In this study, we investigate the role of organic ligands in the photocatalytic conversion of lignin into functionalized aromatics using cadmium sulfide (CdS) quantum dots (QDs). By tuning the hydrophilicity/hydrophobicity of ligands, we successfully form stable QD colloidal solutions, ensuring effective contact between the QDs and lignin. We determined that thiyl ligands triggered the photocatalytic conversion of lignin models. These ligand modifications, including the anchor group and alkyl chain length, are shown to play a critical role in facilitating electron transfer during photocatalysis. Furthermore, it was discovered that the mechanism of C-C and C-O bond cleavage at the β-O-4 linkages can be influenced by the substituents on the aromatic rings of lignin, a finding that has not been previously reported. Our findings not only advance the understanding of ligand-controlled catalysis but also present a new pathway for efficient lignin biomass valorization and organic transformation processes using QD-based photocatalysts.

Introduction

Disrupting the strong reliance on petrochemical compound industry and guarantee sustainable development could only be achieved by establishing a biorefinery model capable of exploiting a complete valorization of lignocellulosic biomass, the largest renewable source of carbon, which is composed of a carbohydrate fraction (cellulose and hemicellulose, up to 70 wt%) and an aromatic-rich polymer fraction (lignin, up to 30 wt%). Both fractions must be valorized, unfortunately, up to now, only the carbohydrate fraction is efficiently repurposed in lignocellulosic biorefineries,[1,2] through pulp manufacturing, whereas a substantial byproduct stream of lignin (technical lignin) is released as a waste, or burnt as low energy fuel, despite being a source of highly desirable aromatic compounds. [3,4]

However, given its distinctive aromatic structure, widespread availability, and low-cost lignin valorization has the potential to serve as a primary alternative to petroleum for producing high-value aromatic compounds. Lignin is made up of three main sub-units *p*-hydroxyphenyl (H), guaiacyl (G) and syringyl (S) crosslinked by C-C and C-O linkages. [5,6] Among them, the β-O-4 ether linkage is the core target of lignin valorization because it is the most abundant and weakest bond, compared to bonds like β-β resinol and 5-5' biphenyl which are more resistant and present greater challenges.[7] However, the β-O-4 availability could be strongly decreased by lignin extraction process, while affecting the depolymerization. Some strategies have employed the *lignin-first* concept, which basically consists of avoiding lignin extraction processes and cleaving the maximum theoretical β-O-4 linkages, directly from milled wood. Unfortunately, the complex mixture of carbohydrate and aromatic products without a trend selectivity makes *lignin-first* difficult to be exploited. Whereas the organosolv technique remains the most effective technique for maintaining β-O-4 bonds and producing clean and faster depolymerization. [2,3]

Controlled and efficient depolymerization of lignocellulose biomass continues being one of the most difficult challenges, current technologies continue employing thermal and chemical catalytic methods, which is not effective due to the high cost and because there is no control on the depolymerization.[8,9] Different approaches have been tested to enhance aromatic monomer production, among them, the "natural way" based on microbial engineering has gained attention for its high selectivity through the specific contact between the lignin bond ligands and the biocatalyst, often composed by enzymes or microorganisms. The performance of this technique is based on boosting the ligand interaction between ligands and the catalytic active center. Unfortunately, it represents cost-effectiveness, poor efficiency and a high-energy-demand technique, however, it represents a good example of ligand triggering depolymerization of lignin. [2,3]

On the other hand, lignin depolymerization via photocatalysis has gained attention for its sustainability and ability to control the depolymerization through regulating different properties on nanomaterial semiconductors such as bandgap, optimal band-edge position, surface area, morphology, etc.[10–13] In addition, it offers advantages such as lower energy requirements, minimal by-products, scalability, and environmental benefits.[14–17] Although there are some studies using photocatalytic routes for lignin depolymerization, there is a lack of interest in determining the effect of nanomaterial ligands and their contribution to depolymerization. This is mainly, since organic ligands on heterogeneous catalyst surfaces, which regulate nucleation and growth kinetics during nanocrystal synthesis, have historically been regarded as deleterious to catalytic efficiency, therefore these organic capping agents are often eliminated through post-synthetic treatments.[18–20] However, some studies have revealed that surface ligands can significantly enhance the performance of nanocatalysts, by acting as mediators and challenging this traditional perspective.[21]

Some researchers have demonstrated that the efficiency of quantum dots (QDs) photocatalysts with organic ligands could enhance the depolymerization based only on the length of ligand and the steric hindrance.[7,22–28] However, research on the role of ligands in photocatalysis for larger molecules remains limited. In this study, CdS quantum dots with various surface ligands are systematically examined for photocatalytic depolymerization of lignin. First, simple lignin models such as benzyl alcohol (BA), and 2-phenoxy-1-phenylethanol (Ppol) were tested to test the catalytic oxidation and the two-step oxidation-

reduction routes. Then a series of dimer lignin models was studied to check the influence of electron-donating groups in the substrate. We demonstrate that catalytic performance is highly influenced by the structure of organic ligands and reveal the mechanism involved by which surface ligands regulate the photocatalytic conversion of lignin. To the best of our knowledge, it represents the first report that demonstrates the activity and selectivity given by ligands agent on nanomaterials photocatalyst, furthermore, By taking advantage of light as a renewable energy source, photocatalysis supports sustainable and circular bioeconomy initiatives to depolymerize lignin into valuable chemicals and monomers.

Results and discussion

CdS quantum dots were synthesized using the conventional hot injection technique with minor changes.[29] Subsequent surface modification and the procedure to obtain all the photocatalyst are provided in the Supporting Information (Table S1). IR spectra (figure S1) allowed to verify the presence of organic bands such as the **ν** O-H and **ν** C=O stretching band characteristic of carboxylic acids, as well as the loss of **ν** C-H stretching characteristic of CdS/OA. The UV/vis technique (figure S2) corroborated that the first excitonic peak of nanocrystals is not affected by ligand exchange. However, a short red-shift was evidenced in the CdS/BF_4 which was attributed to aggregation effects. While TEM images (Figure S3) allowed to verify the presence of nanocrystals of about 3.1 nm for most of the nanocatalysts except for CdS/BF_4, whose diameter was 3.2 nm. However, comparing with the When calculating the particle size using the Peng equation, it was found to be approximately 4.3 nm.[30] This discrepancy in size can be attributed to the fact that solvents in UV/vis spectroscopy can influence the hydrodynamic radius of the particle, thereby leading to an increase in the actual size of the quantum dot. The ^1H NMR technique was used to confirm the presence and attachment of ligands to the surface. Figure S4 demonstrates a distinct shift in the chemical shift of the C-H signal when the ligand is free compared to when it is attached. As an example, for the MPA molecule alone, the two protons from the methylene groups showed a resonance multiplet signal at about 2.63 ppm according with previous reports.[31,32] The formation of the Cd–MPA complex in ligand exchange clearly involves the deprotonation of the thiol group. Compared to the free molecule, the chemical shift and broadening of the two resonance signals indicate the formation of the Cd–MPA complex. The same behavior was observed with the rest of ligands.[33–36] Based on this study, it was estimated the density of ligands on CdS quantum dots. In a standard case using CdS-OA at a concentration of 10 mg/mL, the OA concentration was determined by integrating the alkene resonance in the ^1H NMR spectrum employing 1,2,4,5-tetramethylbenzene as internal standard. This afforded an average 3,62 OA/nm^2 (based on the 4,2 nm of diameter determined by Peng equation). Similarly, the ligand density of mercaptoalkanoic acid ligands was determined using dimethyl sulfone as internal standard (figure S5) and the alkyl hydrogen integration was employed to calculate the density of the associated ligands.[37,38] Apparently, the CdS/MBA presented the higher ligand density with 7,98 MBA/nm^2 which could be produced by π-π stacking. So, the conjugated ligand 4-mercaptobenzoic acid (MBA) could introduce fewer trap states and exhibit a similar charge transfer rate in QD ensembles, but could affect the photocatalytic performance.[39,40]

Photocatalytic conditions are presented in the Supporting Information. **Figure 1** shows the photocatalytic response of the QDs covered with different ligands. First, benzyl alcohol and

2-phenoxyphenylethanol were tested as lignin models compounds to check the ability of photocatalyst to depolymerize lignin. Benzyl alcohol, which has a hydroxyl group in C_α next to aromatic ring, was subjected to oxidation, being quantitatively transformed to benzaldehyde by employing L-Cys, MPA or ME as ligands. A similar behavior was observed when 2-phenoxy-1-phenylethanol, which presents the β-O-4 bond, the target linkage mimicking those present in lignin's structure was employed as substrate, yielding phenol (PhOH) and acetophenone (APO) as major products (scheme S1 and S2 are presented in the Supporting Information, showing the structures of subproducts and conditions of photocatalytic reactions).

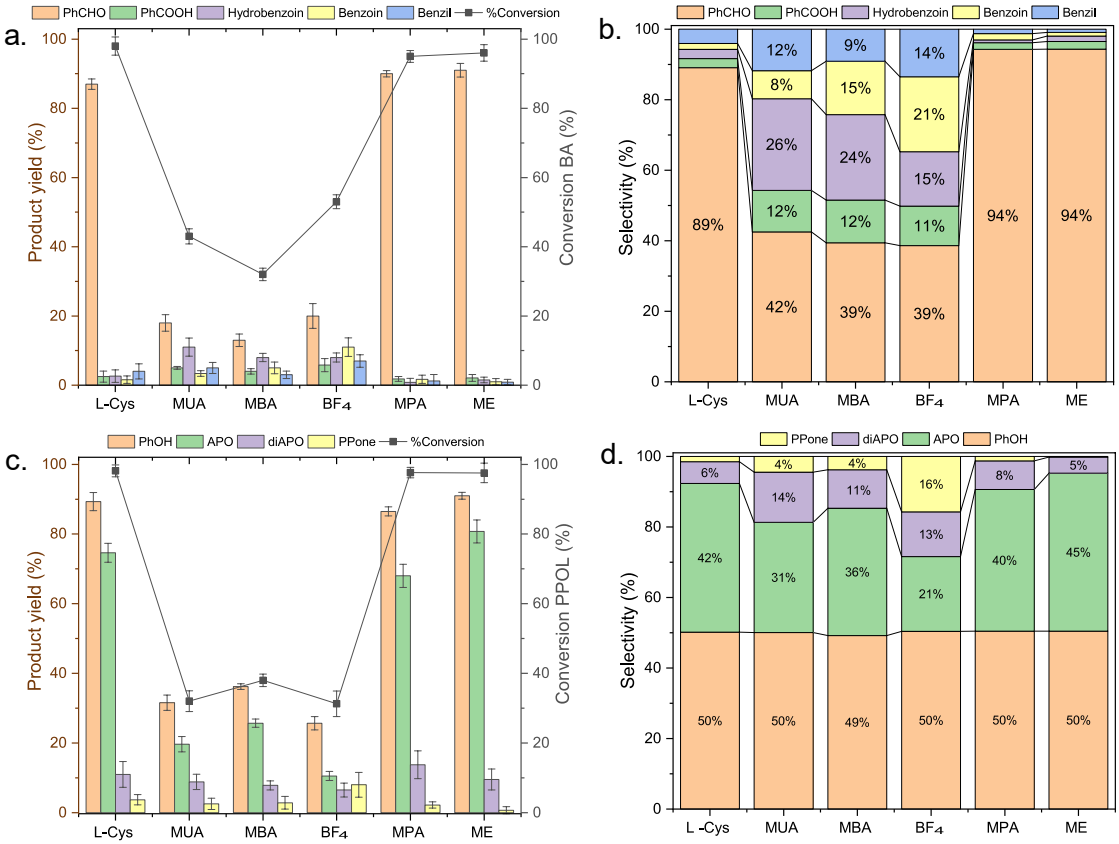

Figure 1. Photocatalytic performances of QDs photocatalyst, employing as substrates benzyl alcohol (yield product and conversion (a) and selectivity (b)) and 2-phenoxyphenyl ethanol (yield product and conversion (c) and selectivity (d))

Different researchers have studied the photo-depolymerization of lignin based on the scission of C-C or C-O involved in the β-O-4 linkage. All of them emphasize that photoinduced holes will attack the C_α-H of the β-O-4 bond of lignin to form C_α radical first this process is known as "oxidative dehydrogenation". Although, some of them consider that the hydroxyl group at the C_α position (C_α-OH) will be dehydrogenated into the carbonyl group (C_α=O) reducing the bond dissociation energy (BDE) of the adjacent C_β-O bond from 69.2

to 55.9 kcal/mol, which makes the subsequent C_β-O bond cleavage much easier, following photocatalytic reduction ensues, but employing two step strategy.[41,42] Recently, it has been reported that after C_α radical formation, electrons can directly or indirectly combine with generated C_α radicals to facilitate the C-O or C-C bonds cleavage.[43] Using this approach, only it is necessary to perform a one-step photoreaction, avoiding separate and purify the generated intermediate ketones, which simplifies the whole reaction.[44] This mechanism was initially observed by Wang et al. using CdS QDs as a photocatalyst.[45] In their experiments with model compounds (2-phenoxy-1-phenyl-ethanol and 2-phenoxy-1-phenylethanone), they discovered that the photocatalytic conversion of a ketone intermediate was notably slow with CdS QDs, suggesting the involvement of an alternative pathway, likely a radical mechanism. DFT calculations showed that generating a C_α radical through interaction with a photogenerated hole significantly reduced the C–O bond dissociation energy (BDE) from 55 to 7.8 kcal/mol, a much greater effect compared to oxidizing C_α–OH to C_α=O.

Similarly, this hypothesis was corroborated in this study by the photocatalytic conversion of the lignin models. First, the CdS/OA (solubilized in *n*-hexane) were tested to oxidize BA, without effective conversion (lower than 5%), indicating a lack of efficiency between the interaction of photogenerated charges and the substrate. These findings clearly demonstrate that adjusting the hydrophilicity and hydrophobicity of ligands in polar or nonpolar solvents to form a QD colloidal solution is crucial for the photocatalytic conversion of lignin models and solid native lignin. The ligand exchange allowed to obtain photocatalyst with mercapto-carboxylic groups which allowed the solubilization of the QDs in polar solvents. The photocatalytic reaction of BA and Ppol, was carried out in a mixture of CH_3CN/H_2O (Supporting information contains details), it was observed that ratio of organic solvent could affect the selectivity of products. Furthermore, the **figures 1a** and **1b**, present the conversion, yield product and selectivity of photoconversion of BA, whereas **Figures 1c** and **1d** show the same behavior but employing Ppol as substrate. Note that in both cases same trend was obtained where the ligands MBA, MUA and BF_4 had the worse conversion. This inefficient performance is closely related to the limitation of photogenerated charges to reach the surface, specifically with mercaptoundecanoic acid (MUA) which has a long aliphatic chain $(CH_2)_{10}$. On the other hand, MBA could stabilize the photogenerated charges due to its conjugated structures that exhibit increased stability due to the delocalization of electrons within π bonds, stabilizing the photogenerated charges by resonance. In contrast, CdS/BF_4, coated by an inorganic anion, should not have the problem of preventing photogenerated charges from reaching the catalyst surface. However, the low conversion of substrate and lack of selectivity remarked that this photocatalyst could suffer aggregation related to the synthetic procedure involved, which required DMF solvent to obtain the colloidal solution of quantum dots.[46,47]

Meanwhile, L-Cys, MPA, and ME ligands demonstrated high conversion and outstanding selectivity. This effectiveness is attributed not only to the short length of the ligands but also to the thiyl radicals that could be generated by photogenerated holes on the quantum dot surfaces. **Figure 1** stablished that the photocatalytic conversion of lignin models was led by the generated thiyl radicals, which were employed to oxidize the BA to benzaldehyde. Whereas in the case of Ppol, the thiyl radicals favor the C_α radical formation by the oxidative hydrogenation, then, the photogenerated electrons produce the reductive bond cleavage. Figure S7, demonstrated the kinetic performance of these ligands with Ppol, showing that in

5 hours of reaction have been reached yield products close to 80% and more than 85% of conversion.

To investigate how the thiyl radicals are involved in the photocatalytic process, different experiments were conducted. **Figure 2A** shows the influence in photoluminescence properties of CdS/OA, when an aliquot of Ppol (0.01 mmol) was added, there was not a drastic change in the fluorescence. However, when the same quantity of MPA (0.01 mmol) was introduced in the cuvette with CdS/OA, a quenching was immediately formed. It means that the photogenerated holes are extracted by the MPA, and there were no recombination effects. So, the 3-mercaptopropionic acid acts as apparent “hole scavenger”. Once confirmed the effect of mercapto-carboxylic ligands on the optical properties of QDs, the presence of radicals produced by photocatalytic study were detected employing DMPO (5,5-dimethyl-1-pyrroline-1-oxide) and HPLC-MS (see Supporting Information). **Figures 2b** and **2c**, showed the adduct created between the C_{α} radical in Ppol and the thiyl radical of MPA, respectively. This experiment confirmed that thiyl radicals were created during the photocatalytic experiment.

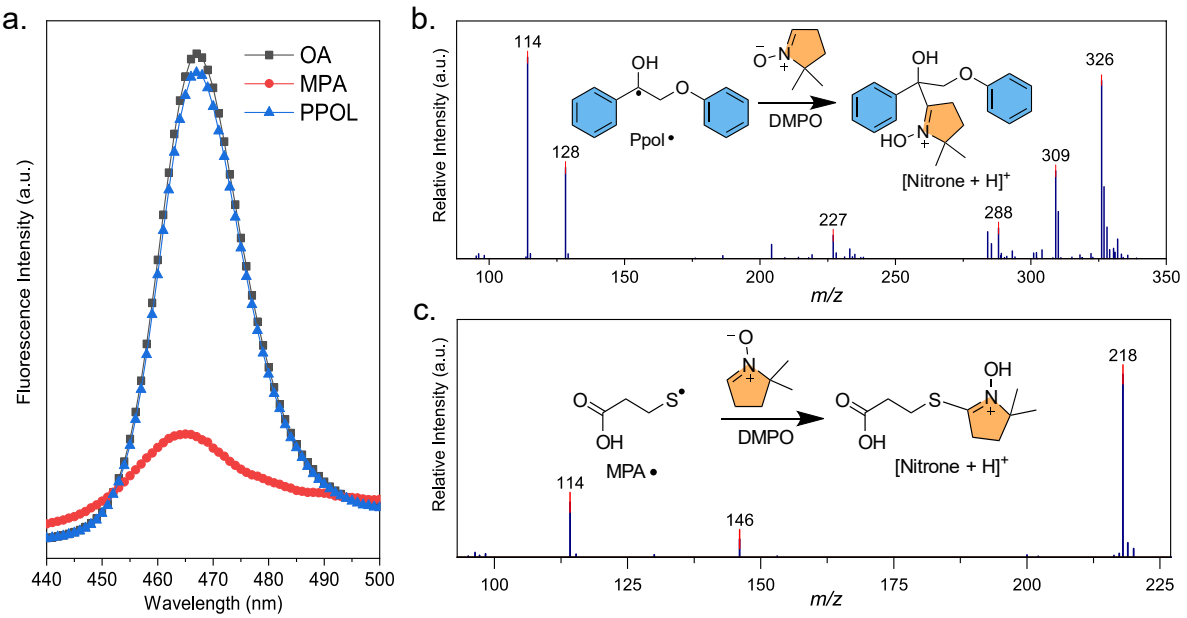

Figure 2. Thiyl radicals study produced during the photocatalytic experiments. Photoluminescence of CdS/OA with addition of 3-mercaptopropionic acid, and 2-phenoxy-1-phenylethanol (a). Detection of Ppol radical (b) and MPA-thiyl radical (c) employing 5,5-dimethyl-1-pyrroline-1-oxide (DMPO).

After corroborating that thiyl radicals were involved in the photocatalytic reaction, different lignin models related to Ppol were tested to check the influence of organic substituents and γ-chain structures. CdS/L-cys was employed as the best photocatalyst to check the reactivity. **Table 1** summarizes the yield product of the compounds obtained by photocatalytic reaction. It was observed that when γ-chain is incorporated in the structure the selectivity of products changed; while the cleavage of the C-O bond is maintained (Table 1, entry 2), when electro-donating groups are incorporated in the aromatic ring, the corresponding aldehydes are obtained. For instance, methoxybenzaldehyde was produced

with 9% of yield product (Table 1, entry 4). Entries 5 and 6 illustrate the conversion observed when three electron-donating groups were introduced into the aromatic ring. Both entries led to the formation of aldehyde compounds, albeit in varying proportions. The presence of a γ-chain resulted in a significant increase in aldehyde yield (22%) compared to the absence of a γ-chain (8%). This suggests a synergistic interaction between the substituents of the lignin monomer model and the γ-chains, influencing the mechanistic pathway of the photocatalyst. Consequently, a combination of cleavages of C-O and C–C bonds in β-O-4 models is demonstrated. However, this hypothesis must be studied employing theoretical calculations and DFT approaches. A simple experimental study was carried out to detect an intermediary capable of producing the aldehyde route. Two lignin model dimers employing 3-methoxy donating group, with and without γ-chain were tested with DMPO to verify the behavior. **Figure 3A** shows the mechanistic route involved in the photocatalytic reactivity. Unfortunately, **Figures 3B** and **3C** revealed that identifying any radical other than the one generated through oxidative dehydrogenation in Cα was not possible. So, although experimental results show a combination of C-C and C-O cleavage pathways for the β-O-4 bond, further studies are required to validate this hypothesis.

Table 1. Lignin model compounds dimers and quantification of compounds obtained by ECN method, see Supporting Information.

Entry	Reactant	Time (h)	Conversion (%)	Yield (%)		
				Ketone	Aldehyde	Phenol
1	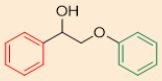	3	98	 (90)	NO detected	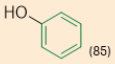 (85)
2	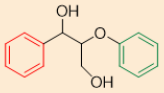	3	97	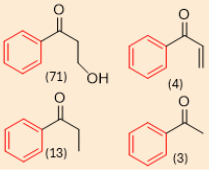 (71) (4) (13) (3)	NO detected	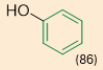 (86)
3	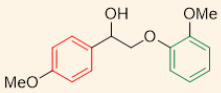	8	93	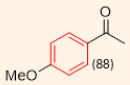 (88)	NO detected	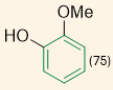 (75)
4	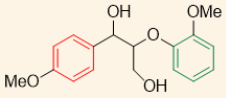	8	88	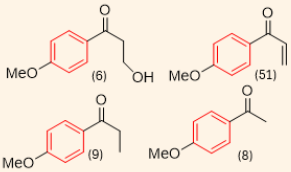 (6) (51) (9) (8)	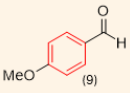 (9)	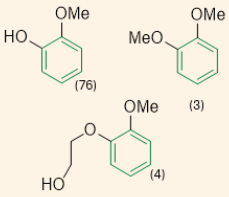 (76) (3) (4)
5	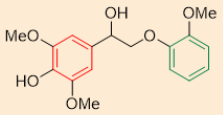	15	93	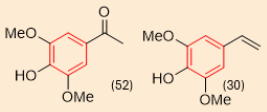 (52) (30)	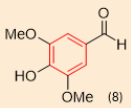 (8)	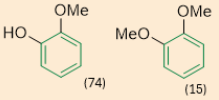 (74) (15)
6	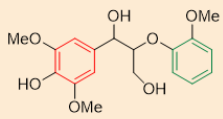	15	75	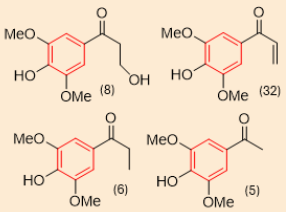 (8) (32) (6) (5)	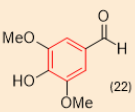 (22)	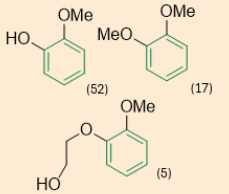 (52) (17) (5)

Based on the results of lignin models, we tested the photocatalytic depolymerization of lignin. First, lignin was extracted from beech wood according to the protocol described in the Supporting Information. (Lignin Beech-EthanoSolv, BES).[48,49] In a typical experiment, 10 mg of BES were added into the test tube reactor and photocatalytic reactions were following according to previous experiments. However, after the reaction was completed, the entire solvent volume was evaporated to dryness using a rotary evaporator. Subsequently, 2 mL of dichloromethane was used to dissolve the monomers. This solution was analyzed by GCMS and GCFID to quantify the monomers obtained. The unreacted lignin was studied by 2D-HSQC method. **Figure 4** shows the spectra obtained for aliphatic and aromatic region. The most prominent result was the disappearance of the aliphatic signals associated with the β-O-4 bond.[50,51] The structures molecules in blue represent the contributions of C_α-H, C_β-H and C_γ-H. It was determined that the C_γ-H suffered littles changes, which means that there are remanent fragments unreacted after photocatalytic reactions.

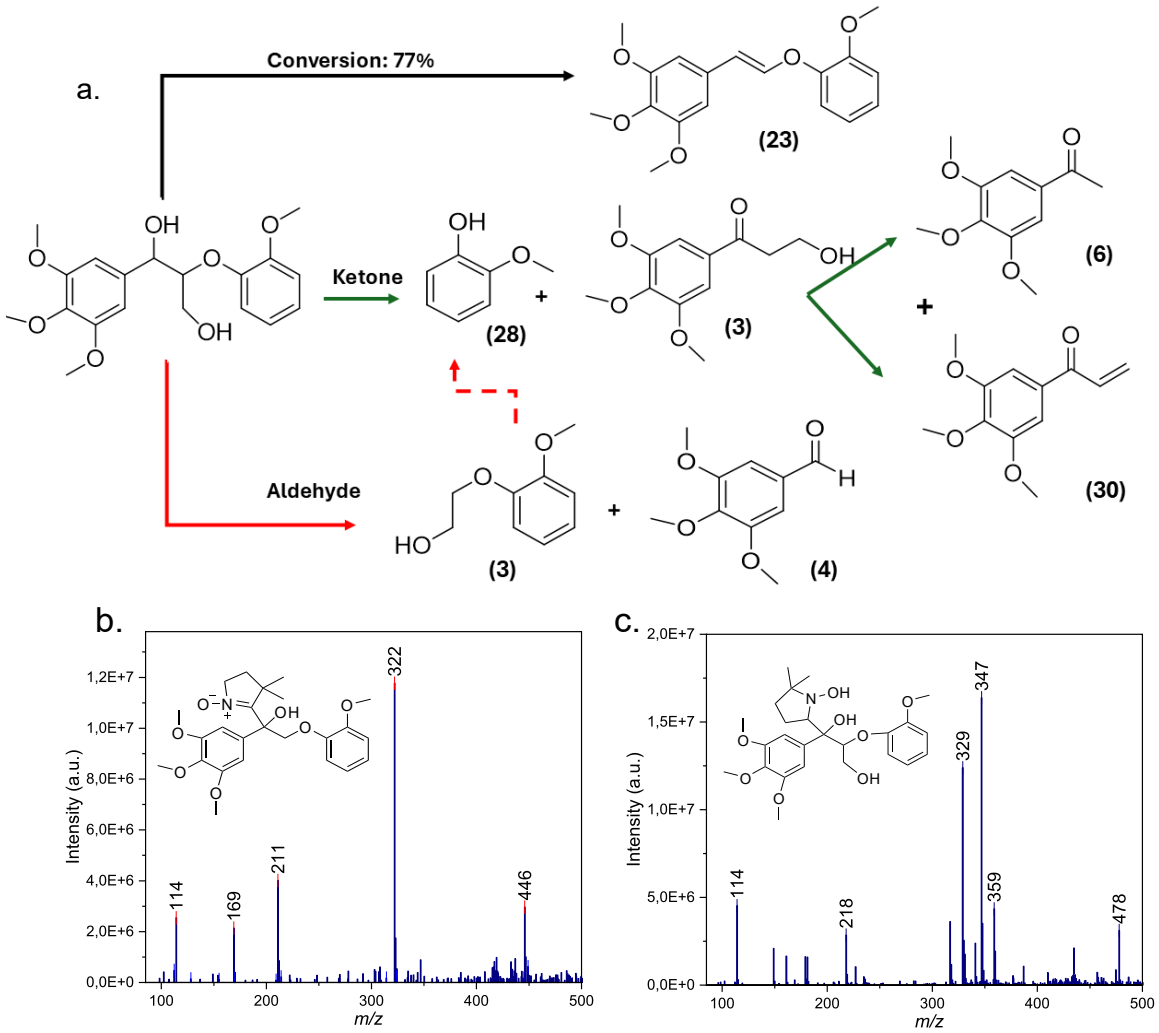

Figure 3. (a) Possible reaction pathways routes to evaluate reactivity between detection of radicals of lignin dimer without γ-chains (b) and with γ-chains (c).

Similarly, in the aliphatic region, signals corresponding to phenyl coumarin and resinol units remained unchanged during the photocatalytic reaction, indicating that photocatalysis was effective only in cleaving β-O-4 bonds. Additionally, the aromatic region (**Figure 4c** and **4d**) shows a reduction in signal contributions, which may suggest a loss of conjugation. This results in distinct signals corresponding to non-conjugated molecules that are more accessible, representing monomers. Similarly, although the signal covers a smaller area, it exhibits higher intensity.[51]

Another way to confirm the cleavage of β-O-4 bonds is by using a semiquantitative 2D-HSQC method.[37,45] By analyzing the ^{13}C-^{1}H cross-signal assignments (Table S4), it was possible to correlate the aliphatic region with aromatic signals associated with β-O-4 bonds. Figure S10 displays the integral zone linked to these signals. This approach allowed us to estimate the theoretical maximum monomer yield. Table S6 shows that prior to the reaction, the theoretical maximum monomer yield was 17.5%, whereas after the reaction, only 2.1% bonds remained, indicating that the photocatalytic reaction achieved an 88% monomer yield conversion.

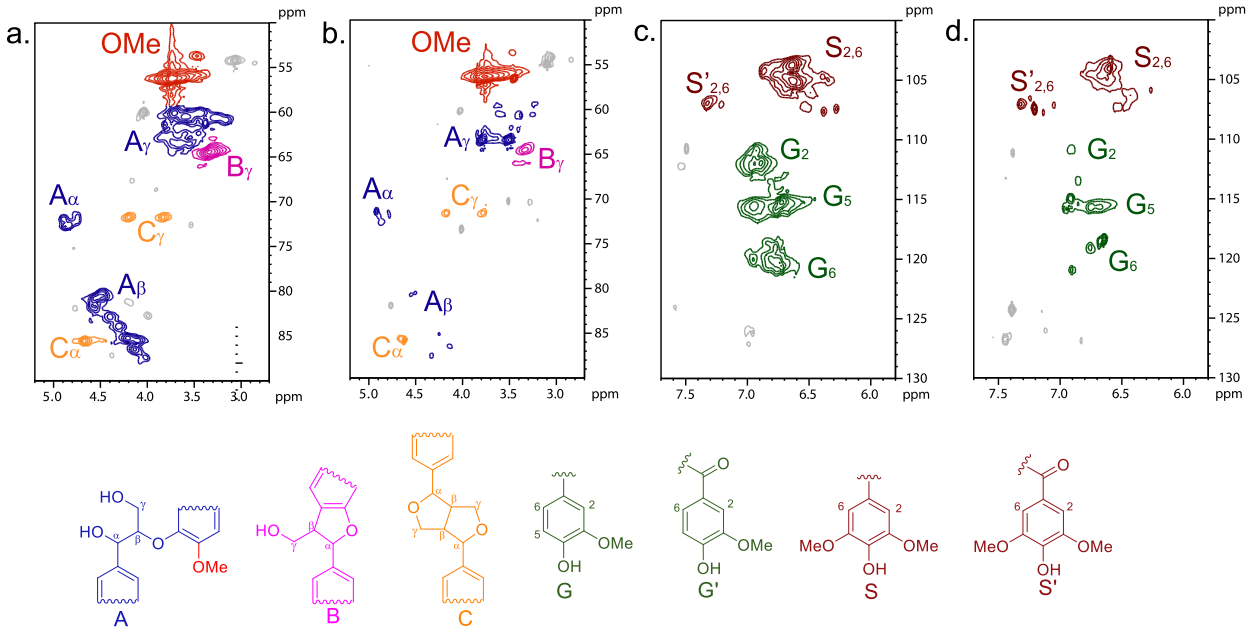

Figure 4. 2D HSQC NMR spectrum of birch woodmeal. Before (a,c) and after reaction (b,d). Aα, Aβ and Aγ denote the C−H in α, β and γ carbons of β-O-4 linkages. Bα, Bβ and Bγ denote the C−H in α, β and γ carbons of phenylcoumaran units. Cα, Cβ and Cγ denote the C−H α, β and γ carbons of retinol units

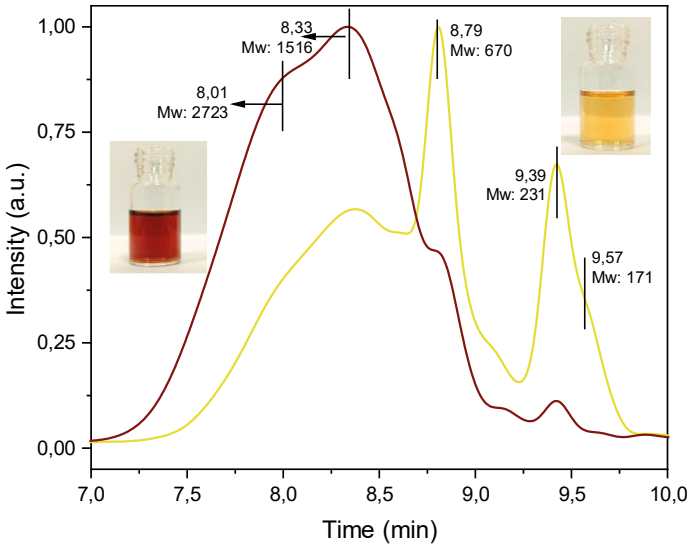

Figure 5. Gel permeation chromatography of lignin beech ethanosolv before (brown line) and after photocatalytic reaction (yellow line)

A more accurate method to quantify monomer yield is by using calibration curves for the major monomers produced, vanillin and syringaldehyde (Figure S11). This aligns with the results obtained for the lignin model compound, suggesting that the mechanistic pathway may change when the substrate is highly condensed and contains electron-donating groups. Various tests were conducted to ensure the reproducibility of lignin BES depolymerization (Table S7), yielding 2.97% for vanillin and 4.30% for syringaldehyde. To assess monomer production efficiency, the nitrobenzene oxidation (NBO) method, also known as alkaline nitrobenzene oxidation (AN oxidation), was applied to analyze the total monomers present before the BES reaction. Table S7 shows a maximum monomer yield of 4.1% w/w for vanillin and 4.7% w/w for syringaldehyde. By comparing the total amount of vanillin and syringaldehyde produced after photocatalytic reactions to the total monomers initially present, the experimental monomer yield was determined to be 82.6%. This result closely aligns with the semi-quantitative values obtained using 2D-HSQC. These findings confirm that the efficiency of monomer production exceeds 80%

The production of monomers and lignin depolymerization can also be analyzed using gel permeation chromatography (Figure 5). Initially, before the reaction, lignin was predominantly composed of macrostructures (Mw = 1516). However, after the reaction, most of these structures were converted into trimers consisting of 3-4 monomer subunits (Mw = 670). Additionally, monomers with molecular weights around 231 and 171 were detected, which are likely associated with the production of vanillin and syringaldehyde.

In summary, this research demonstrated the vital role of semiconducting QD ligands in the photocatalytic conversion of lignin, driven by thiyl-mediated ligands. It underlines the importance of regulating not only the hydrophilic or hydrophobic properties of organic ligands, which influence dispersion and colloidal stability, but also enabling charge transfer from the QD core to the catalytic surface. Furthermore, the study found that electron-donating groups in lignin model compounds can significantly impact the mechanistic pathway of photocatalysis, which has been studied by theoretical DFT studies to identify the

underlying mechanisms. This work confirms that photocatalytic lignin conversion enhances the production of high monomer yields and functionalized aromatics.

Acknowledgements

N.G. thanks the support from grant “Ramon y Cajal” (RYC2018-023888-I) funded by MCIN/AEI/10.13039/501100011033. Likewise, N.G. wants to acknowledge the support received *via* the grants CNS2023-145354 and PID2021-128805NA-I00 funded by MCIN/AEI/10.13039/501100011033 and by the “European Union Next Generatio-nEU/PRTR”. X.M. wants to acknowledge the support received *via* Spanish Ministerio de Ciencia e Innovación (PID2021-127332NB-100). This project has also received funding from the European Research Council (ERC) under the European Union’s Horizon 2020 research and innovation program (grant agreement No.948829).

References

1. Zhou, C.-H., Xia, X., Lin, C.-X., Tong, D.-S. & Beltramini, J. Catalytic conversion of lignocellulosic biomass to fine chemicals and fuels. *Chem Soc Rev* **40**, 5588–5617 (2011).
2. Liao, J. C., Mi, L., Pontrelli, S. & Luo, S. Fuelling the future: microbial engineering for the production of sustainable biofuels. *Nat Rev Microbiol* **14**, 288–304 (2016).
3. Feldmeier, K. & Höcker, B. Computational protein design of ligand binding and catalysis. *Curr Opin Chem Biol* **17**, 929–933 (2013).
4. Cordes, M. & Giese, B. Electron transfer in peptides and proteins. *Chem Soc Rev* **38**, 892–901 (2009).
5. Huang, W., Hua, Q. & Cao, T. ChemInform Abstract: Influence and Removal of Capping Ligands on Catalytic Colloidal Nanoparticles. *ChemInform* **45**, (2014).
6. Cordes, M. & Giese, B. Electron transfer in peptides and proteins. *Chem Soc Rev* **38**, 892–901 (2009).
7. Liu, P., Qin, R., Fu, G. & Zheng, N. Surface Coordination Chemistry of Metal Nanomaterials. *J Am Chem Soc* **139**, 2122–2131 (2017).
8. Wu, X. *et al.* Ligand-Controlled Photocatalysis of CdS Quantum Dots for Lignin Valorization under Visible Light. *ACS Catal* **9**, 8443–8451 (2019).
9. Wu, X. *et al.* Solar energy-driven lignin-first approach to full utilization of lignocellulosic biomass under mild conditions. *Nat Catal* **1**, 772–780 (2018).
10. Vasudevan, D., Gaddam, R. R., Trinchi, A. & Cole, I. Core-Shell Quantum Dots: Properties and Applications. *J Alloys Compd* (2015) doi:10.1016/j.jallcom.2015.02.102.

11. Zhang, J. *et al.* Semicondutor quantum dots-based metal ion. **2**, 43–64 (2014).

12. Mitsuru Ishikawa, V. B. Chapter 2 - Luminescent Quantum Dots, Making Invisibles Visible in Bioimaging. in *Progress in Molecular Biology and Translational Science* 53–99 (2011).

13. Murphy, C. J. & Coffer, J. L. *Quantum Dots: APrimer*. *16A* vol. 56 (2002).

14. Dorfs, D. *et al. Quantum Dots: Synthesis and Characterization*. *Comprehensive Nanoscience and Nanotechnology* vol. 1 (Elsevier Ltd., 2011).

15. R. W. Knoss. *Quantum Dots: Research, Technology and Applications*. *Quantum Dots: Research, Technology and Applications* (2008).

16. Reshma, V. G. & Mohanan, P. V. Quantum dots: Applications and safety consequences. *Journal of Luminescence* vol. 205 287–298 Preprint at https://doi.org/10.1016/j.jlumin.2018.09.015 (2019).

17. Gidwani, B. *et al.* Quantum dots: Prospectives, toxicity, advances and applications. *Journal of Drug Delivery Science and Technology* vol. 61 Preprint at https://doi.org/10.1016/j.jddst.2020.102308 (2021).

18. Querner, C., Reiss, P., Bleuse, J. & Pron, A. Chelating ligands for nanocrystals' surface functionalization. *J Am Chem Soc* **126**, 11574–11582 (2004).

19. Green, M. The nature of quantum dot capping ligands. *J Mater Chem* **20**, 5797 (2010).

20. Zhou, J., Liu, Y., Tang, J. & Tang, W. Surface ligands engineering of semiconductor quantum dots for chemosensory and biological applications. *Biochem Pharmacol* **20**, 360–376 (2017).

21. Rosen, E. L. *et al.* Exceptionally Mild Reactive Stripping of Native Ligands from Nanocrystal Surfaces by Using Meerwein's Salt. *Angewandte Chemie International Edition* **51**, 684–689 (2012).

22. Salami, R., Zeng, Y., Han, X., Rohani, S. & Zheng, Y. Exploring catalyst developments in heterogeneous CO2 hydrogenation to methanol and ethanol: A journey through reaction pathways. *Journal of Energy Chemistry* **101**, 345–384 (2025).

23. Schoenbaum, C. A., Schwartz, D. K. & Medlin, J. W. Controlling the Surface Environment of Heterogeneous Catalysts Using Self-Assembled Monolayers. *Acc Chem Res* **47**, 1438–1445 (2014).

24. Pang, S. H., Schoenbaum, C. A., Schwartz, D. K. & Medlin, J. W. Directing reaction pathways by catalyst active-site selection using self-assembled monolayers. *Nat Commun* **4**, 2448 (2013).

25. Marshall, S. T. *et al.* Controlled selectivity for palladium catalysts using self-assembled monolayers. *Nat Mater* **9**, 853–858 (2010).

26. Zhao, X. *et al.* Thiol Treatment Creates Selective Palladium Catalysts for Semihydrogenation of Internal Alkynes. *Chem* **4**, 1080–1091 (2018).

27. Chen, G. *et al.* Interfacial electronic effects control the reaction selectivity of platinum catalysts. *Nat Mater* **15**, 564–569 (2016).

28. Schrader, I., Warneke, J., Backenköhler, J. & Kunz, S. Functionalization of Platinum Nanoparticles with l-Proline: Simultaneous Enhancements of Catalytic Activity and Selectivity. *J Am Chem Soc* **137**, 905–912 (2015).

29. Yu, W. W. & Peng, X. Formation of High-Quality CdS and Other II–VI Semiconductor Nanocrystals in Noncoordinating Solvents: Tunable Reactivity of Monomers. *Angewandte Chemie International Edition* **41**, 2368–2371 (2002).

30. Yu, W. W., Qu, L., Guo, W. & Peng, X. Experimental determination of the extinction coefficient of CdTe, CdSe, and CdS nanocrystals. *Chemistry of Materials* **15**, 2854–2860 (2003).

31. Wan, W. *et al.* Room-temperature formation of CdS magic-size clusters in aqueous solutions assisted by primary amines. *Nat Commun* **11**, 4199 (2020).

32. Böhm, M. L. *et al.* Size and Energy Level Tuning of Quantum Dot Solids via a Hybrid Ligand Complex. *J Phys Chem Lett* **6**, 3510–3514 (2015).

33. Kuznetsova, V. A. *et al.* Effect of Chiral Ligand Concentration and Binding Mode on Chiroptical Activity of CdSe/CdS Quantum Dots. *ACS Nano* **13**, 13560–13572 (2019).

34. Hens, Z. & Martins, J. C. A solution NMR toolbox for characterizing the surface chemistry of colloidal nanocrystals. *Chemistry of Materials* vol. 25 1211–1221 Preprint at https://doi.org/10.1021/cm303361s (2013).

35. Kroupa, D. M. *et al.* Tuning colloidal quantum dot band edge positions through solution-phase surface chemistry modification. *Nat Commun* **8**, 15257 (2017).

36. Fritzinger, B., Capek, R. K., Lambert, K., Martins, J. C. & Hens, Z. Utilizing Self-Exchange To Address the Binding of Carboxylic Acid Ligands to CdSe Quantum Dots. *J Am Chem Soc* **132**, 10195–10201 (2010).

37. Wu, X. *et al.* Ligand-Controlled Photocatalysis of CdS Quantum Dots for Lignin Valorization under Visible Light. *ACS Catal* **9**, 8443–8451 (2019).

38. Fisher, A. A. E., Osborne, M. A., Day, I. J. & Lucena Alcalde, G. Measurement of ligand coverage on cadmium selenide nanocrystals and its influence on dielectric dependent photoluminescence intermittency. *Commun Chem* **2**, (2019).

39. dos Santos, J. A. L. *et al.* 3-Mercaptopropionic, 4-Mercaptobenzoic, and Oleic Acid-Capped CdSe Quantum Dots: Interparticle Distance, Anchoring Groups, and Surface Passivation. *J Nanomater* **2019**, 2796746 (2019).

40. Liang, Y., Thorne, J. E. & Parkinson, B. A. Controlling the Electronic Coupling between CdSe Quantum Dots and Thiol Capping Ligands via pH and Ligand Selection. *Langmuir* **28**, 11072–11077 (2012).

41. Han, G. *et al.* Highly Selective Photocatalytic Valorization of Lignin Model Compounds Using Ultrathin Metal/CdS. *ACS Catal* **9**, 11341–11349 (2019).

42. Zhu, G. *et al.* Depolymerization of lignin by microwave-assisted methylation of benzylic alcohols. *Bioresour Technol* **218**, 718–722 (2016).

43. Hou, T. *et al.* Yin and Yang Dual Characters of CuOx Clusters for C–C Bond Oxidation Driven by Visible Light. *ACS Catal* **7**, 3850–3859 (2017).

44. Wu, X. *et al.* Photocatalytic transformations of lignocellulosic biomass into chemicals. *Chem Soc Rev* **49**, 6198–6223 (2020).

45. Wu, X. *et al.* Solar energy-driven lignin-first approach to full utilization of lignocellulosic biomass under mild conditions. *Nat Catal* **1**, 772–780 (2018).

46. Rosen, E. L. *et al.* Exceptionally Mild Reactive Stripping of Native Ligands from Nanocrystal Surfaces by Using Meerwein's Salt. *Angewandte Chemie International Edition* **51**, 684–689 (2012).

47. Chang, C. M., Orchard, K. L., Martindale, B. C. M. & Reisner, E. Ligand removal from CdS quantum dots for enhanced photocatalytic H2 generation in pH neutral water. *J Mater Chem A Mater* **4**, 2856–2862 (2016).

48. Zijlstra, D. S. *et al.* Mild Organosolv Lignin Extraction with Alcohols: The Importance of Benzylic Alkoxylation. *ACS Sustain Chem Eng* **8**, 5119–5131 (2020).

49. Schulze, P., Seidel-Morgenstern, A., Lorenz, H., Leschinsky, M. & Unkelbach, G. Advanced process for precipitation of lignin from ethanol organosolv spent liquors. *Bioresour Technol* **199**, 128–134 (2016).

50. Wu, X. *et al.* Ligand-Controlled Photocatalysis of CdS Quantum Dots for Lignin Valorization under Visible Light. *ACS Catal* **9**, 8443–8451 (2019).

51. Talebi Amiri, M., Bertella, S., Questell-Santiago, Y. M. & Luterbacher, J. S. Establishing lignin structure-upgradeability relationships using quantitative 1H–13C heteronuclear single quantum coherence nuclear magnetic resonance (HSQC-NMR) spectroscopy. *Chem Sci* **10**, 8135–8142 (2019).